



Pseudorapidity dependence of the anisotropic flow of charged particles in Pb–Pb collisions at $\sqrt{s_{\text{NN}}} = 2.76 \text{ TeV}$

ALICE Collaboration^{1,*}

ARTICLE INFO

Article history:

Received 17 May 2016

Received in revised form 21 June 2016

Accepted 6 July 2016

Available online 11 July 2016

Editor: L. Rolandi

ABSTRACT

We present measurements of the elliptic (v_2), triangular (v_3) and quadrangular (v_4) anisotropic azimuthal flow over a wide range of pseudorapidities ($-3.5 < \eta < 5$). The measurements are performed with Pb–Pb collisions at $\sqrt{s_{\text{NN}}} = 2.76 \text{ TeV}$ using the ALICE detector at the Large Hadron Collider (LHC). The flow harmonics are obtained using two- and four-particle correlations from nine different centrality intervals covering central to peripheral collisions. We find that the shape of $v_n(\eta)$ is largely independent of centrality for the flow harmonics $n = 2–4$, however the higher harmonics fall off more steeply with increasing $|\eta|$. We assess the validity of extended longitudinal scaling of v_2 by comparing to lower energy measurements, and find that the higher harmonic flow coefficients are proportional to the charged particle densities at larger pseudorapidities. Finally, we compare our measurements to both hydrodynamical and transport models, and find they both have challenges when it comes to describing our data.

© 2016 The Author. Published by Elsevier B.V. This is an open access article under the CC BY license (<http://creativecommons.org/licenses/by/4.0/>). Funded by SCOAP³.

1. Introduction

The main goal of the heavy-ion physics program at the Large Hadron Collider (LHC) is to study the quark-gluon plasma (QGP), a deconfined state of matter existing at extreme temperatures and energy-densities. Experimental results from RHIC were the first to suggest that the QGP behaves as a nearly perfect fluid [1–4]. A particularly important observable when characterizing the QGP is anisotropic azimuthal flow. The anisotropic flow develops from pressure gradients originating from the initial spatial geometry of a collision and is observed as a momentum anisotropy in the final-state particles. It is usually described by flow harmonics, which are defined as the Fourier coefficients:

$$v_n = \langle \cos[n(\varphi - \Psi_n)] \rangle, \quad (1)$$

where n is the order of the flow harmonic, φ is the azimuthal angle and Ψ_n is the symmetry plane angle of harmonic n . The first three Fourier coefficients, v_1 , v_2 , and v_3 are known as directed, elliptic and triangular flow, respectively. The flow harmonics v_1 to v_6 have been studied extensively at RHIC [1–7] and the LHC [8–17]. The observed anisotropic flow is considered to be a strong indication of collectivity [18] and is described well by relativistic hydrodynamics [19].

Anisotropic flow studies at RHIC played a major role in establishing that the produced system is a strongly interacting quark-gluon plasma (sQGP) [1–4] with a shear viscosity to entropy density ratio (η/s) close to the conjectured lower limit of $1/(4\pi)$ predicted by the AdS/CFT correspondence [20]. The fact that higher order harmonics are increasingly suppressed by viscosity [21] makes it possible to use anisotropic flow measurements to estimate the η/s of the produced system [22,23].

The pseudorapidity (η) dependence of the flow harmonics can play a key role in understanding the temperature dependence of η/s , something that can be determined using Quantum Chromodynamics (QCD) [24–26]. At forward rapidities, the average temperature drops which implies η/s will also change. In addition, the lower temperatures at forward rapidities mean the system will spend less time in the QGP phase leading to the hadronic viscosity playing a greater role in affecting the flow harmonics [26,27]. Recently, it has been suggested that the symmetry plane angles may depend on η [28–30]. While this effect is not directly studied in this Letter, considering that the reference particles are taken from mid-rapidity, the measured values of anisotropy coefficients at forward rapidity will be suppressed if the symmetry-plane angles fluctuate with η .

At RHIC, the PHOBOS experiment reported the pseudorapidity dependence of elliptic flow over a wide range ($-5.0 < \eta < 5.3$) and variety of collision energies [31–33], and system sizes [34]. It was found that in the rest frame of one of the colliding nuclei ($\eta - y_{\text{beam}}$), v_2 is energy independent. This feature was also ob-

¹ See Appendix A for the list of collaboration members.

* E-mail address: alice-publications@cern.ch.

served in multiplicity density distributions [35,36] and for v_1 [37]. This suggests that at forward rapidity, in the fragmentation region, particle production is independent of the collision energy, an effect known as extended longitudinal scaling.

In this Letter, we present measurements of v_2 , v_3 , and v_4 over a wide pseudorapidity range ($-3.5 < \eta < 5.0$) in Pb–Pb collisions at $\sqrt{s_{\text{NN}}} = 2.76$ TeV using the ALICE detector. At the LHC, the pseudorapidity dependence of the flow harmonics has already been reported by ATLAS [12,38] and CMS [13,16] in a limited η -range ($|\eta| < 2.5$ and $|\eta| < 2.4$, respectively). The extended longitudinal scaling has been shown to hold for multiplicity densities [39] and directed flow [15], and appears to occur for elliptic flow [13,38]. Here, the η -range is extended considerably compared to the former results and we will investigate whether the extended longitudinal scaling of elliptic flow continues to hold. We will compare our data to hydrodynamical and transport models, and investigate the decrease of v_n in the forward regions relative to $dN_{\text{ch}}/d\eta$.

2. Experimental setup

A detailed description of the ALICE detector is available elsewhere [40]. In this section, the sub-detectors used in this analysis are described: the V0 detector, the Time Projection Chamber (TPC), the Inner Tracking System (ITS) and the Forward Multiplicity Detector (FMD). The V0 detector consists of 2 arrays of scintillators located on opposite sides of the interaction point (IP) along the beam line. The detector has full azimuthal coverage in the ranges of $2.8 < \eta < 5.1$ (V0-A) and $-3.7 < \eta < -1.7$ (V0-C) [41]. The detector acts as an online trigger and, with its large coverage, as a centrality estimator.

Charged particle tracks are reconstructed using the TPC, a large Time Projection Chamber [42]. The detector can provide position and momentum information. Particles that traverse the TPC volume leave ionization trails that drift towards the endcaps, where they are detected. Full length tracks can be reconstructed in the range $|\eta| < 0.8$. For this analysis, a transverse momentum range of $0.2 < p_T < 5.0$ GeV/c was used. To ensure good track quality, the tracks are required to have at least 70 reconstructed TPC space points (cluster) out of 159 possible and an average χ^2 per TPC cluster ≤ 4 . In addition, to reduce contamination from secondary particles (weak decays or interactions with material), a cut on the distance of closest approach (DCA) between the track and the primary vertex is applied both in the transverse plane ($\text{DCA}_{xy} < 2.4$ cm) and on the z-coordinate ($\text{DCA}_z < 3.2$ cm).

The ITS is made up of six cylindrical concentric silicon layers divided into three sub-systems, the Silicon Pixel Detector (SPD), the Silicon Drift Detector (SDD) and the Silicon Strip Detector (SSD), each consisting of two layers [40]. ITS clusters can be combined with the TPC information to improve track resolution. The SPD has additional applications [40]. Firstly, it is used to estimate the primary vertex as it is located close to the beam pipe. Secondly, clusters from the SPD inner layer, which consists of 3.3×10^6 pixels of size $50 \times 425 \mu\text{m}^2$, are used to estimate the number of charged particles in the range $|\eta| < 2.0$.

The FMD consists of five silicon rings, providing a pseudorapidity coverage in the ranges $-3.5 < \eta < -1.7$ and $1.7 < \eta < 5.0$ [43]. The rings are single-layer detectors and only charged particle hits, not tracks, are measured. This means that primary and secondary particles cannot be distinguished. There are two types of FMD rings: inner ring and outer rings. Inner rings have 512 radial strips each covering 18° in azimuth and outer rings have 256 radial strips each covering 9° in azimuth. The charged particle estimation in the FMD is described in more detail elsewhere [39]. The inner layer of the SPD and the five FMD rings allow one to measure charged particle hits in the range $-3.5 < \eta < 5.0$.

3. Data sample and analysis details

We analysed 10 million minimum bias Pb–Pb collisions at $\sqrt{s_{\text{NN}}} = 2.76$ TeV. The sample was recorded during the first LHC heavy-ion data-taking period in 2010. A minimum-bias trigger requiring a coincidence between the signals from V0-A and V0-C was used. In addition, it is required that the primary vertex, determined by the SPD, be within $|v_z| < 10.0$ cm, where $v_z = 0$ cm is the location of the nominal interaction position. The measurements are grouped according to fractions of the inelastic cross section, and cover the 80% most central collisions. The V0 detector is used for the centrality estimate which is described in more detail elsewhere [44]. For the most central to the most peripheral events, the V0 has a centrality resolution of 0.5% to 2%, respectively.

The flow harmonics are estimated using the Q-cumulants method [45] for two- and four-particle correlations, denoted as $v_n\{2\}$ and $v_n\{4\}$ respectively. The two- and four-particle cumulants respond differently to flow fluctuations. The two-particle cumulants are enhanced, while four-particle cumulants are suppressed. At forward rapidities, the pseudorapidity density is relatively low. This means that it is not always possible to get statistically significant results using only particles from a small region in η . To circumvent this using the Q-cumulants method, the reference flow measurement is performed using the charged particle tracks from the TPC, where the correlations at mid-rapidity are measured. As a systematic check, the charged particle tracks using a combination of the TPC and ITS are also used. Then, for the $v_n(\eta)$ analysis, the correlations between charged particle hits (from the SPD or FMD) and the tracks are measured in η -bins 0.5 units of pseudorapidity wide. To avoid autocorrelations between the SPD clusters and tracks, the tracks for the reference particles are located in a different η -region than the SPD hits. Effectively, for SPD hits with $\eta < 0$, tracks are required to have $\eta > 0$ and vice versa. The same considerations apply for FMD hits. Due to the use of particle hits, only the p_T -integrated flow is measured. The ϕ distribution for the SPD or FMD clusters is not uniform, therefore a non-uniform acceptance correction is applied based on relations derived elsewhere [46].

As the inner rings of the FMD have only 20 azimuthal segments, the flow harmonics are slightly suppressed. The effect of this was recently calculated [47] and found to be 1.6%, 3.7% and 6.5% for v_2 , v_3 and v_4 respectively. This suppression is taken into account in the final results. When using charged particle hits it is not possible to distinguish secondary particles (from material interactions and decays) from primary particles. For the regions covered by the SPD, the contamination from secondary particles is small (< 10%), as the inner layer of the SPD is very close to the beam pipe. Away from mid-rapidity, in the FMD, dense material such as cooling tubes and read-out cables cause a very large production of secondary particles – up to twice the number of primary particles according to Monte Carlo (MC) studies. These secondary particles are deflected in ϕ with respect to the mother particle, which causes a reduction in the observed flow. The reduction of flow caused by the secondary particles is estimated using an event generator containing particle yields, ratios, momentum spectra and flow coefficients, which are then subject to a full detector simulation using GEANT3 [48]. To make sure that the correction is not model dependent, the AMPT MC event generator [49,50] is used as an independent input, with GEANT3 again used to model the detector response. Using these simulations, the reduction is found to be larger for higher harmonics, up to 41% for v_4 . Finally, the correction also accounts for missing very low p_T particles, which increase the observed v_n as these particles have a very small v_n . However, as the correction is always less than 1, the dominant effect comes from the secondary particles, which reduce v_n .

Few-particle correlations, not originating from the initial geometry termed non-flow (decays, jets, etc.), enhance the two-particle cumulant measurements. The non-flow contribution to the four-particle cumulant is found to be negligible [45,51], however, it is necessary to apply a correction to the two-particle cumulant. In the FMD and SPD, there is also a non-flow contribution from secondary particles, as they are sometimes produced in pairs. For the differential flow measurement, there is a rapidity-gap between the charged particle hits and the charged particle tracks. For the SPD, it is between 0 and 2 units in pseudorapidity, while for the FMD it is between 0.9 and 4.2 units in pseudorapidity. The large rapidity gap suppresses the non-flow contribution at forward rapidity. However, at mid-rapidities, this contribution is non-negligible and needs appropriate corrections. For the reference flow measurement there is no rapidity gap, and non-flow removal is important. For this analysis, the non-flow contributions are estimated using the HIJING event generator [52] and GEANT3 for the detector simulation. The non-flow contribution is estimated and subtracted separately for the reference and differential flow, before the correction for the deflection of secondary particles is applied and the v_n estimates are derived.

4. Systematic uncertainties

Numerous sources of systematic uncertainty were investigated, including effects due to detector cuts, choice of reference particles and uncertainties related to the secondary particle correction. Four major contributors to the systematic uncertainty were identified: the choice of reference tracks, the model dependence of the secondary particle correction, the description of the detector used for the simulations, and finally the non-flow correction. As the non-flow contribution to the four-particle cumulant is negligible, only the first three systematic uncertainties are considered for $v_2\{4\}$. The systematic uncertainties assigned to each of the sources are shown in Table 1, and are described in more detail below.

The dependence of the differential flow on the reference tracks was tested by using tracks with combined information from the TPC and ITS, rather than tracks with only TPC information. The systematic uncertainty from the choice of reference tracks was found to vary slightly with centrality, with the most central events having the largest uncertainty. To test the model dependence of secondary particle production, the correction from the toy-model described above is compared to the one derived from AMPT tuned to LHC data. Both the secondary particle correction and the non-flow correction derived from HIJING are sensitive to inaccuracies in the description of the detector used for the simulation. To test this sensitivity, the output of two HIJING simulations with a flow afterburner, one with +7% material density and one with -7% material density, are compared to the output from having normal material density. In this case the systematic uncertainty has a small η -dependence, as there are significantly fewer secondary particles at mid-rapidity. The 3% uncertainty is applicable to the SPD, while the 4% uncertainty is applicable to the FMD.

We assessed the systematic uncertainty associated with the non-flow correction in two ways. Firstly, following another method proposed to subtract non-flow [53], the two-particle cumulants were obtained from minimum bias pp collisions, where it is assumed that there is negligible anisotropic flow. The pp reference and differential cumulants are then rescaled according to their multiplicity, M , using the ratio $M^{\text{pp}}/M^{\text{cent}}$, then subtracted from the corresponding A-A cumulants. Any differences found between this method and the default HIJING method are treated as systematic uncertainties. Secondly, by using only charged particle hits from the SPD and FMD, it is possible to construct a two-particle cumulant with a large rapidity-gap, $v_n\{2, |\Delta\eta| > 2.0\}$,

Table 1
List of the systematic uncertainties for each observable.

Source	$v_2\{2\}$	$v_3\{2\}$	$v_4\{2\}$	$v_2\{4\}$
Reference particle tracks	2–4%	2–4%	2–6%	2–4%
Model dependence	5%	5%	7%	5%
Material budget	3–4%	3–4%	3–4%	3–4%
Non-flow correction	2–10%	2–10%	2–10%	-
Total	6–12%	6–13%	6–14%	6–8%

which largely removes all non-flow contributions. Unfortunately, this observable is statistically stable only for v_2 and v_3 , so it is used as a further cross check. In Table 1, the 2% uncertainties correspond to mid-central collisions where the ratio of flow to non-flow is largest, while the 10% uncertainties correspond to very central and very peripheral collisions where the ratio of flow to non-flow is smallest. Finally, we used the AMPT model [49,50] to investigate if there are differences between $v_n(\eta)$ and $v_n(y)$, as η is supposed to approximate y . We found there are 15% differences in the flow coefficients at mid-rapidity, which reduced to 0% for $\eta > 2$. We did not assign any systematic uncertainties due to these differences, as we are explicitly reporting measurements as a function of η (as in the case of $dN_{\text{ch}}/d\eta$ measurements).

The systematic uncertainty assigned to the non-flow correction is the largest contributor to the total systematic uncertainty, except for $v_2\{4\}$ due to the four-particle cumulant's insensitivity to non-flow. The total systematic uncertainties are slightly dependent on centrality and pseudorapidity.

5. Results

An overview of the four observables in each centrality class is shown in Fig. 1. Due to the changing overlap geometry, a strong centrality dependence of the elliptic flow is observed over the entire pseudorapidity range. The weaker centrality dependence of the higher order coefficients v_3 and v_4 is an indication that initial-state fluctuations play a prominent role, as the centrality dependence of the corresponding eccentricities are more modest relative to $n = 2$ [21]. The different behaviour of $v_2\{2\}$ and $v_2\{4\}$ caused by flow fluctuations is also clearly seen. For the most peripheral events, there are not enough particles to get statistically stable results for $v_2\{4\}$ and similarly for $v_4\{2\}$ due to the relatively small quadrangular flow.

The p_T -integrated elliptic flow was also measured by CMS [13] and ATLAS [38] in Pb-Pb collisions at $\sqrt{s_{\text{NN}}} = 2.76$ TeV and by PHOBOS in Au-Au collisions at $\sqrt{s_{\text{NN}}} = 200$ GeV [32]. A comparison between those results and this analysis is shown for the 25–50% centrality class in Fig. 2. In the common region of pseudorapidity acceptance, the results of present analysis are consistent with the results obtained by CMS and ATLAS experiments within the systematic uncertainties. The present analyses extends the measurements to a wider range of pseudorapidity. The values of v_2 at all pseudorapidities measured at LHC energies are larger than the corresponding values at RHIC, as reported by PHOBOS. This increase in elliptic flow coincides with a larger p_T at the LHC energy [8].

The extended longitudinal scaling observed by PHOBOS in Au-Au collisions with centre-of-mass energies from 19.6 to 200 GeV [33] is found to hold up to the LHC energy (shown in Fig. 3). This is consistent with what was found by CMS [13] and ATLAS [38]. Here it is shown as an event average for the 0–40% most central events. The event average means that the analysis was performed in smaller centrality bins using multiplicity weights, and was then averaged over the centrality bins using the number of events as a weight [45]. To examine boost invariance, it would be preferable to

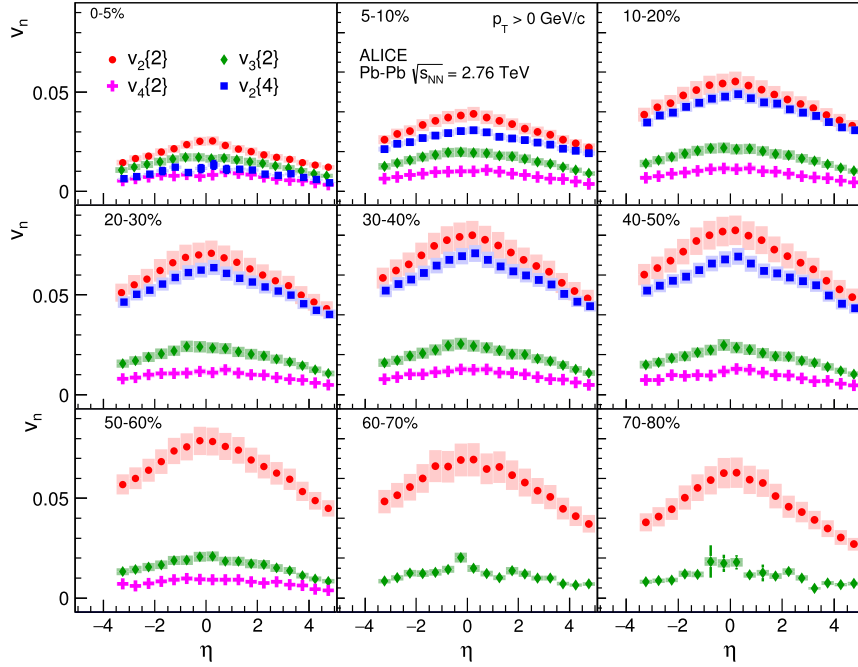


Fig. 1. Measurements of the pseudorapidity dependence of v_2 , v_3 and v_4 in each centrality bin. The vertical lines represent the statistical uncertainties and the boxes represent the systematic uncertainties. The statistical uncertainties are usually smaller than the marker size.

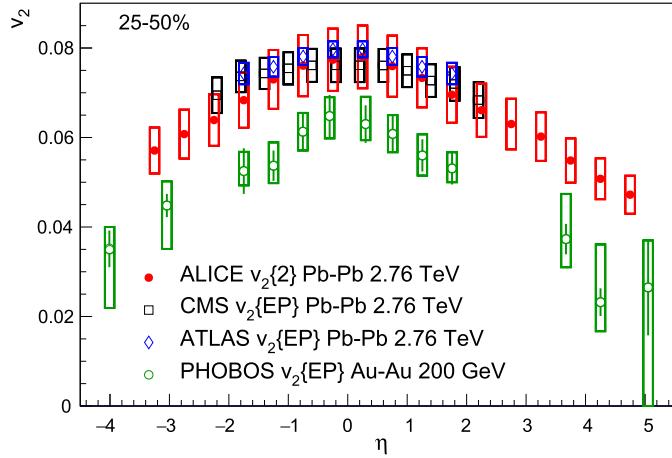


Fig. 2. Elliptic flow for the 25–50% centrality range. Boxes represent systematic uncertainties and errors bars represent statistical uncertainties. The results for $v_2\{2\}$ from this analysis are compared to measurements using the event plane method from CMS [13] and ATLAS [38] at the same energy and lower energy results from PHOBOS [32]. For the comparable LHC energy, the p_T range for ALICE is $p_T > 0$ GeV/c, for CMS is $0.3 < p_T < 3$ GeV/c, and for ATLAS is $p_T > 0.07$ GeV/c.

use rapidity (y) instead of pseudorapidity, unfortunately that is not possible using the FMD as the momentum cannot be measured.

PHOBOS found the shape of $v_2(\eta)$ to be largely independent of centrality, with only the overall level changing between central and peripheral events [32]. The ratios of central to peripheral events for v_2 , v_3 and v_4 using the two-particle cumulant are shown in Fig. 4. Here it is observed that none of the harmonics show a clear centrality dependence in the shape of $v_n(\eta)$ within uncertainties (albeit hints of such a dependence are present in the v_2 ratio), consistent with the results from PHOBOS at lower energy.

It is known that the suppression from viscous effects to the flow harmonics increases with n [21]. The hadronic phase is speculated to be more dominant at forward rapidity [26,27]. Therefore, the relative decrease of the flow harmonics may help to disentangle

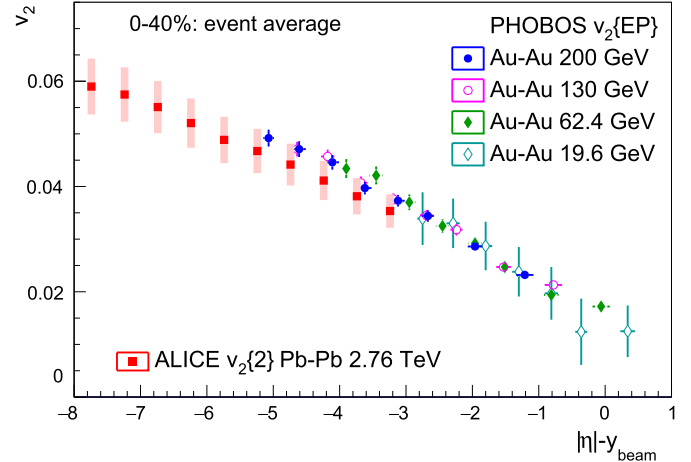


Fig. 3. The elliptic flow as observed in the rest frame of one of the projectiles by using the variable $|\eta| - y_{beam}$ ($y_{beam} = 7.99$) for the event averaged 0–40% centrality. The results from $v_2\{2\}$ from this analysis are compared to lower energy results from PHOBOS [33]. The vertical lines represent the statistical uncertainties and the boxes represent the systematic uncertainties. For the PHOBOS results only statistical errors are shown.

the viscous effects from the hadronic phase with those from the QGP phase. When the ratio v_m/v_n ($n \neq m$) is formed most of the common systematic uncertainties cancel, leaving the contribution from the non-flow correction. The ratios of v_3/v_2 and v_4/v_3 are shown for the 30–40% most central events in Fig. 5. A small decrease with $|\eta|$ is observed for v_3/v_2 , qualitatively consistent with the expectation from viscous effects suppressing higher harmonics. The v_4/v_3 ratio remains constant with $|\eta|$ within the uncertainties. The figure also shows v_4/v_2^2 , which is commonly used to estimate the non-linear contribution to v_4 from the elliptic anisotropy [5]. Given the uncertainties, it is difficult to conclude whether v_4/v_2^2 changes with respect to $|\eta|$.

As mentioned previously, at forward rapidities the steepness of $v_n(\eta)$ has been linked to the hadronic contribution to the vis-

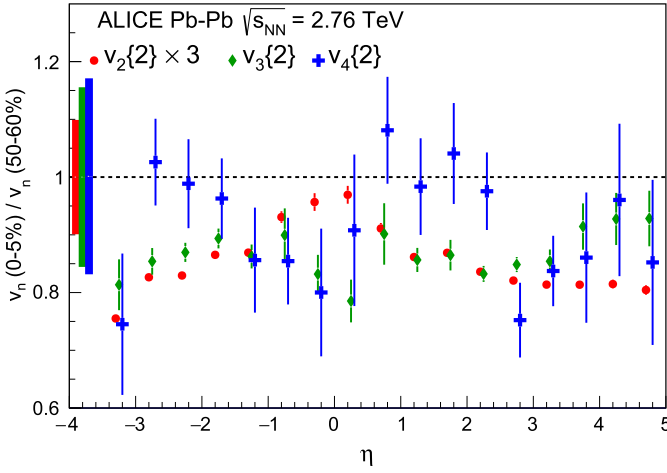


Fig. 4. Ratio of $v_n\{2\}$ between central (0–5%) and peripheral (50–60%) events for v_2 , v_3 and v_4 . The vertical lines represent the statistical uncertainties and the boxes represent the systematic uncertainties. The v_2 results are multiplied by 3 to fit on the same scale as v_3 and v_4 .

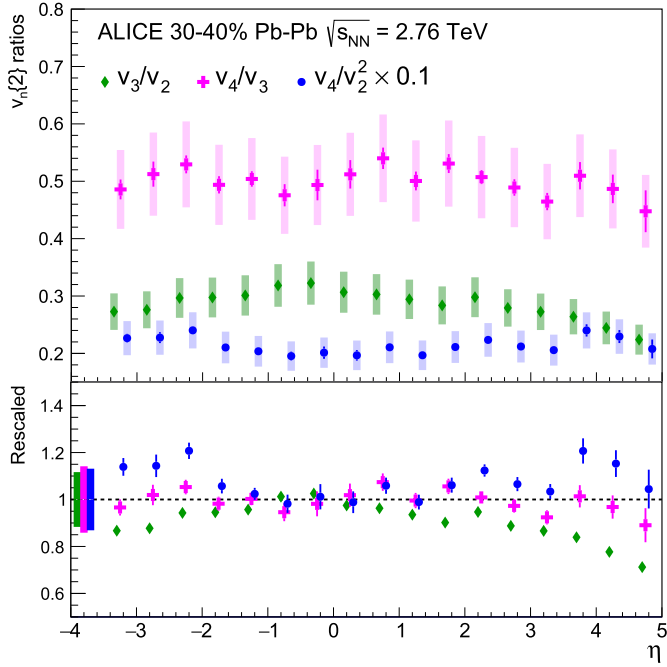


Fig. 5. Ratios between different harmonics for the 30–40% centrality range. The vertical lines represent the statistical uncertainties and the boxes represent the common systematic uncertainties. In the bottom panel the ratios are rescaled to 1 at mid-rapidity and the common systematic uncertainties are shown as the thick bars on the left.

cosy to entropy ratio [26,27]. The larger the hadronic η/s , the steeper the fall off. We also note that the pseudorapidity densities of charged particles decrease in this region. In order to investigate the correspondence of the latter, in Fig. 6 we show the ratio of various v_n coefficients to previous ALICE measurements of $dN_{ch}/d\eta$ [39]. In order to avoid any influence of the Jacobian translation from y to η , only the range $\eta > 2$ is shown. We find that this ratio is generally flat, with the exception of v_2 at the larger values of η . This indicates that within a fixed centrality interval, v_3 and v_4 are largely driven by the local particle density. Indeed, when comparing p-Pb and Pb-Pb collisions at LHC energies, it was found that values of $v_3\{2\}$ were similar for similar values of $dN_{ch}/d\eta$ [51]. The correlation found between both quantities may be sim-

ply attributed to the fact that both particle production and the development of anisotropic flow are driven by the number of interactions in the system.

In Fig. 7, we compare our data to hydrodynamic calculations tuned to RHIC data [26]. The tuning involves finding a parameterization of the temperature dependence of η/s , so that the hydrodynamical calculations describe PHOBOS measurements of $v_2(\eta)$ [32,33]. It is clear that the same parameterization does not describe the LHC data as well. For both centralities, the elliptic flow coefficient v_2 is generally underestimated, while the higher order coefficients v_3 and v_4 are generally overestimated. This points to the need for an either an alternative parameterization of η/s that describes both the RHIC and LHC data simultaneously, or further investigations into whether the initial state model used is applicable for the LHC energies.

In contrast to hydrodynamical models, AMPT is a non-equilibrium model that attempts to simulate parton production after the initial collision, and collective behaviour arises from parton and hadronic rescatterings. It has previously been tuned to agree with ALICE measurements of v_2 vs. p_T and multiplicity for the 40–50% most central events. It was found to reproduce $v_3(p_T)$ well using the same parameters. In Fig. 8 the results of this analysis are compared to the output of the AMPT model for two different centralities. For the centrality range of 40–50%, which AMPT is tuned to match, there is good agreement at mid-rapidity for all observables modulo $v_2\{4\}$ at larger $|\eta|$, where AMPT underestimates the data. The underestimation at forward rapidity is found to be independent of the choice of reference particles, suggesting that it is unrelated to symmetry plane angle fluctuations with η . For more central events AMPT tends to overestimate flow at forward rapidities, except for v_4 which it describes quite well over the entire range. At mid-rapidity AMPT agrees with the observed values of v_2 , v_3 and v_4 within the systematic uncertainties. Further tuning may lead to an improvement at forward rapidities, and should be investigated in future studies.

6. Conclusions

The pseudorapidity dependence of the anisotropic flow harmonics v_2 , v_3 and v_4 have been measured in Pb-Pb collisions at $\sqrt{s_{NN}} = 2.76$ TeV using the ALICE detector. The measurement is performed over the widest η -range at the LHC, $-3.5 < \eta < 5.0$, in nine centrality bins covering 0 to 80% of the total inelastic cross section. It was found that the shape of $v_n(\eta)$ does not depend obviously on centrality. Comparing to lower energy measurements at RHIC, elliptic flow is larger at the LHC over the entire pseudorapidity range and extended longitudinal scaling of v_2 observed at lower collision energies is still valid up to the LHC energy. In the range $|\eta| < 2.5$ the results were found to be consistent with previous LHC measurements. At forward rapidities, the higher harmonic flow coefficients are proportional to the charged particle densities for a given centrality, while the ratio of v_2 to $dN_{ch}/d\eta$ rises with increasing η . A comparison to hydrodynamic calculations tuned to RHIC data has difficulties in describing our data in some η regions, and this suggests that the LHC data play a key role in constraining either the temperature dependence of η/s or the initial state. Finally, comparing our data to AMPT, the model describes the flow well at mid-rapidity, but fails for v_2 at forward rapidities.

Acknowledgements

The ALICE Collaboration would like to thank all its engineers and technicians for their invaluable contributions to the construction of the experiment and the CERN accelerator teams for the outstanding performance of the LHC complex. The ALICE Collaboration

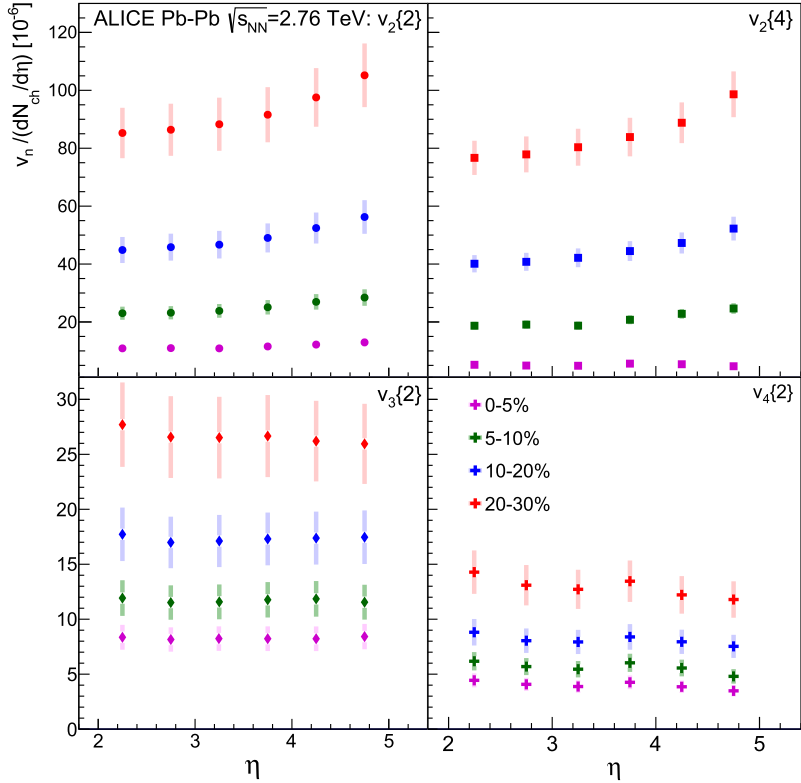


Fig. 6. Ratios between v_n coefficients and $dN_{ch}/d\eta$ values for different centralities. Measurements of $dN_{ch}/d\eta$ are taken from a previous ALICE publication [39]. Only systematic uncertainties are shown, as the statistical uncertainties are smaller than the symbols.

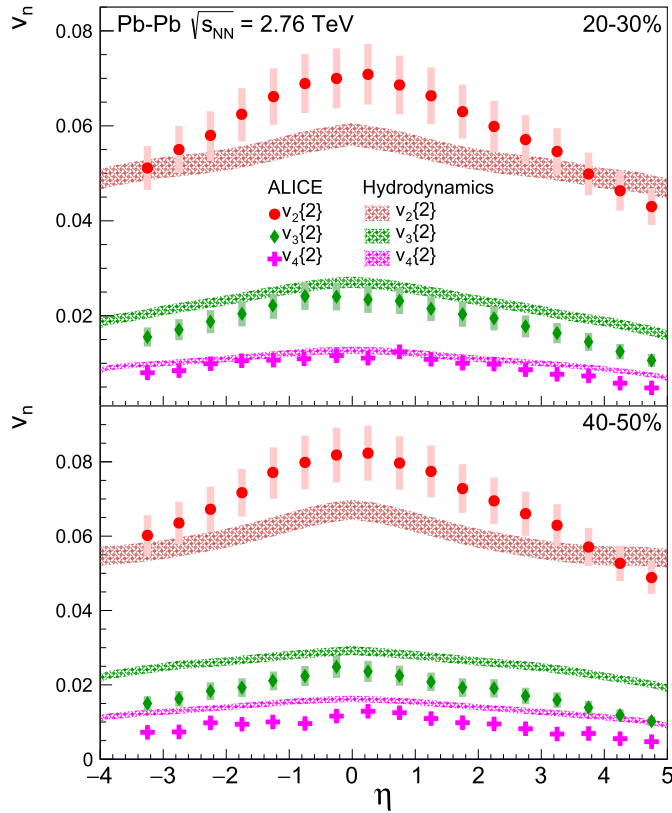


Fig. 7. Comparisons to hydrodynamics predictions [26], where input parameters (temperature dependence of η/s) have been tuned to RHIC data for the Pb-Pb 20–30% (top) and 40–50% (bottom) centralities. The predictions are for Pb-Pb $\sqrt{s_{NN}} = 2.76$ TeV collisions.

gratefully acknowledges the resources and support provided by all Grid centres and the Worldwide LHC Computing Grid (WLCG) collaboration. The ALICE Collaboration acknowledges the following funding agencies for their support in building and running the ALICE detector: State Committee of Science, World Federation of Scientists (WFS) and Swiss Fonds Kidagan, Armenia; Conselho Nacional de Desenvolvimento Científico e Tecnológico (CNPq), Financiadora de Estudos e Projetos (FINEP), Fundação de Amparo à Pesquisa do Estado de São Paulo (FAPESP); Ministry of Science & Technology of China (MSTC), National Natural Science Foundation of China (NSFC) and Ministry of Education of the People's Republic of China (MOEC); Ministry of Science, Education and Sports of Croatia and Unity through Knowledge Fund, Croatia; Ministry of Education, Youth and Sports of the Czech Republic; Danish Natural Science Research Council, the Carlsberg Foundation and the Danish National Research Foundation; The European Research Council under the European Community's Seventh Framework Programme; Helsinki Institute of Physics and the Academy of Finland; French CNRS-IN2P3, the 'Region Pays de Loire', 'Region Alsace', 'Region Auvergne' and CEA, France; German Bundesministerium für Bildung und Forschung (BMBF) and the Helmholtz Association; General Secretariat for Research and Technology, Ministry of Development, Greece; National Research, Development and Innovation Office (NKFIH), Hungary; Council of Scientific and Industrial Research (CSIR), New Delhi; Department of Atomic Energy, Government of India and Department of Science and Technology of the Government of India; Instituto Nazionale di Fisica Nucleare (INFN) and Centro Fermi – Museo Storico della Fisica e Centro Studi e Ricerche "Enrico Fermi", Italy; Japan Society for the Promotion of Science (JSPS) KAKENHI and MEXT, Japan; National Research Foundation of Korea (NRF); Consejo Nacional de Ciencia y Tecnología (CONACYT), Dirección General de Asuntos del Personal Académico, Universidad Nacional Autónoma de México (DGAPA), Amérique

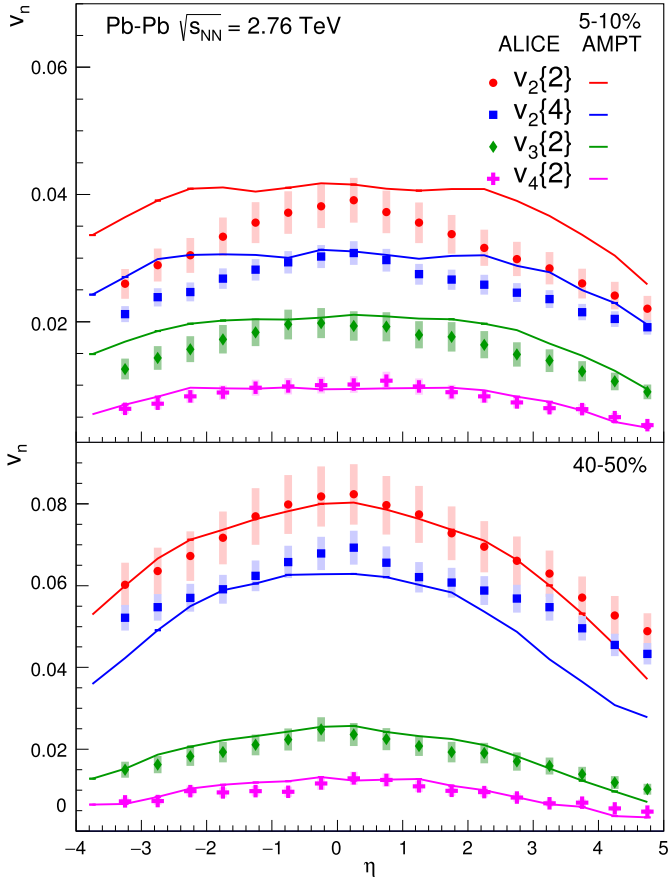


Fig. 8. Comparison to AMPT [49,50] for the centrality ranges 5–10% and (top) and 40–50% (bottom). The AMPT predictions are for Pb–Pb $\sqrt{s_{NN}} = 2.76$ TeV collisions.

Latine Formation Academique – European Commission (ALFA-EC) and the EPLANET Program (European Particle Physics Latin American Network); Stichting voor Fundamenteel Onderzoek der Materie (FOM) and the Nederlandse Organisatie voor Wetenschappelijk Onderzoek (NWO), Netherlands; Research Council of Norway (NFR); Pontificia Universidad Católica del Perú; National Science Centre, Poland; Ministry of National Education/Institute for Atomic Physics and National Council of Scientific Research in Higher Education (CNCI-UEFISCDI), Romania; Joint Institute for Nuclear Research, Dubna; Ministry of Education and Science of Russian Federation, Russian Academy of Sciences, Russian Federal Agency of Atomic Energy, Russian Federal Agency for Science and Innovation and The Russian Foundation for Basic Research; Ministry of Education, Science, Research and Sport of the Slovak Republic; Department of Science and Technology, Republic of South Africa; Centro de Investigaciones Energeticas, Medioambientales y Tecnologicas (CIEMAT), E-Infrastructure shared between Europe and Latin America (EELA), Ministerio de Economía y Competitividad (MINECO) of Spain, Xunta de Galicia (Consellería de Educación), Centro de Aplicaciones Tecnológicas y Desarrollo Nuclear (CEADEN), Cubaenergía, Cuba, and IAEA (International Atomic Energy Agency); Swedish Research Council (VR) and Knut and Alice Wallenberg Foundation (KAW); National Science and Technology Development Agency (NSTDA), Suranaree University of Technology (SUT) and Office of the Higher Education Commission under NRU project of Thailand; Ministry of Education and Science of Ukraine; United Kingdom Science and Technology Facilities Council (STFC); The U.S. Department of Energy, the United States National Science Foundation, the State of Texas Attorney General, and the State of Ohio.

References

- [1] BRAHMS Collaboration, I. Arsene, et al., Quark gluon plasma and color glass condensate at RHIC? The perspective from the BRAHMS experiment, *Nucl. Phys. A* 757 (2005) 1–27, arXiv:nucl-ex/0410022.
- [2] PHOBOS Collaboration, B. Back, M. Baker, M. Ballintijn, D. Barton, B. Becker, et al., The PHOBOS perspective on discoveries at RHIC, *Nucl. Phys. A* 757 (2005) 28–101, arXiv:nucl-ex/0410022.
- [3] STAR Collaboration, J. Adams, et al., Experimental and theoretical challenges in the search for the quark gluon plasma: the STAR Collaboration's critical assessment of the evidence from RHIC collisions, *Nucl. Phys. A* 757 (2005) 102–183, arXiv:nucl-ex/0501009.
- [4] PHENIX Collaboration, K. Adcox, et al., Formation of dense partonic matter in relativistic nucleus–nucleus collisions at RHIC: experimental evaluation by the PHENIX Collaboration, *Nucl. Phys. A* 757 (2005) 184–283, arXiv:nucl-ex/0410003.
- [5] STAR Collaboration, J. Adams, et al., Azimuthal anisotropy at RHIC: the first and fourth harmonics, *Phys. Rev. Lett.* 92 (2004) 062301, arXiv:nucl-ex/0310029.
- [6] PHENIX Collaboration, A. Adare, et al., Measurements of higher-order flow harmonics in Au + Au collisions at $\sqrt{s_{NN}} = 200$ GeV, *Phys. Rev. Lett.* 107 (2011) 252301, arXiv:1105.3928 [nucl-ex].
- [7] STAR Collaboration, L. Adamczyk, et al., Third harmonic flow of charged particles in Au + Au collisions at $\sqrt{s_{NN}} = 200$ GeV, *Phys. Rev. C* 88 (1) (2013) 014904, arXiv:1301.2187 [nucl-ex].
- [8] ALICE Collaboration, K. Aamodt, et al., Elliptic flow of charged particles in Pb–Pb collisions at 2.76 TeV, *Phys. Rev. Lett.* 105 (2010) 252302, arXiv:1011.3914 [nucl-ex].
- [9] ALICE Collaboration, K. Aamodt, et al., Higher harmonic anisotropic flow measurements of charged particles in Pb–Pb collisions at $\sqrt{s_{NN}} = 2.76$ TeV, *Phys. Rev. Lett.* 107 (2011) 032301, arXiv:1105.3865 [nucl-ex].
- [10] ATLAS Collaboration, G. Aad, et al., Measurement of the pseudorapidity and transverse momentum dependence of the elliptic flow of charged particles in lead–lead collisions at $\sqrt{s_{NN}} = 2.76$ TeV with the ATLAS detector, *Phys. Lett. B* 707 (2012) 330–348, arXiv:1108.6018 [hep-ex].
- [11] CMS Collaboration, S. Chatrchyan, et al., Centrality dependence of dihadron correlations and azimuthal anisotropy harmonics in PbPb collisions at $\sqrt{s_{NN}} = 2.76$ TeV, *Eur. Phys. J. C* 72 (2012) 2012, arXiv:1201.3158 [nucl-ex].
- [12] ATLAS Collaboration, G. Aad, et al., Measurement of the azimuthal anisotropy for charged particle production in $\sqrt{s_{NN}} = 2.76$ TeV lead–lead collisions with the ATLAS detector, *Phys. Rev. C* 86 (2012) 014907, arXiv:1203.3087 [hep-ex].
- [13] CMS Collaboration, S. Chatrchyan, et al., Measurement of the elliptic anisotropy of charged particles produced in PbPb collisions at $\sqrt{s_{NN}} = 2.76$ TeV, *Phys. Rev. C* 87 (2013) 014902, arXiv:1204.1409 [nucl-ex].
- [14] ATLAS Collaboration, G. Aad, et al., Measurement of the distributions of event-by-event flow harmonics in lead–lead collisions at 2.76 TeV with the ATLAS detector at the LHC, *J. High Energy Phys.* 1311 (2013) 183, arXiv:1305.2942 [hep-ex].
- [15] ALICE Collaboration, B. Abelev, et al., Directed flow of charged particles at midrapidity relative to the spectator plane in Pb–Pb collisions at $\sqrt{s_{NN}} = 2.76$ TeV, *Phys. Rev. Lett.* 111 (23) (2013) 232302, arXiv:1306.4145 [nucl-ex].
- [16] CMS Collaboration, S. Chatrchyan, et al., Measurement of higher-order harmonic azimuthal anisotropy in PbPb collisions at $\sqrt{s_{NN}} = 2.76$ TeV, *Phys. Rev. C* 89 (2014) 044906, arXiv:1310.8651 [nucl-ex].
- [17] ALICE Collaboration, B.B. Abelev, et al., Elliptic flow of identified hadrons in Pb–Pb collisions at $\sqrt{s_{NN}} = 2.76$ TeV, *J. High Energy Phys.* 06 (2015) 190, arXiv:1405.4632 [nucl-ex].
- [18] J.-Y. Ollitrault, Anisotropy as a signature of transverse collective flow, *Phys. Rev. D* 46 (1992) 229–245.
- [19] M. Luzum, P. Romatschke, Conformal relativistic viscous hydrodynamics: applications to RHIC results at $\sqrt{s_{NN}} = 200$ GeV, *Phys. Rev. C* 78 (2008) 034915, arXiv:0804.4015 [nucl-th].
- [20] P. Kovtun, D.T. Son, A.O. Starinets, Viscosity in strongly interacting quantum field theories from black hole physics, *Phys. Rev. Lett.* 94 (2005) 111601, arXiv:hep-th/0405231.
- [21] B.H. Alver, C. Gombeaud, M. Luzum, J.-Y. Ollitrault, Triangular flow in hydrodynamics and transport theory, *Phys. Rev. C* 82 (2010) 034913, arXiv:1007.5469 [nucl-th].
- [22] M. Luzum, J.-Y. Ollitrault, Extracting the shear viscosity of the quark–gluon plasma from flow in ultra-central heavy-ion collisions, *Nucl. Phys. A* 904–905 (2013) 377c–380c, arXiv:1210.6010 [nucl-th].
- [23] F.G. Gardim, J. Noronha-Hostler, M. Luzum, F. Grassi, Effects of viscosity on the mapping of initial to final state in heavy ion collisions, *Phys. Rev. C* 91 (3) (2015) 034902, arXiv:1411.2574 [nucl-th].
- [24] M. Prakash, M. Prakash, R. Venugopalan, G. Welke, Nonequilibrium properties of hadronic mixtures, *Phys. Rep.* 227 (1993) 321–366.
- [25] P.B. Arnold, G.D. Moore, L.G. Yaffe, Transport coefficients in high temperature gauge theories. 2. Beyond leading log, *J. High Energy Phys.* 05 (2003) 051, arXiv:hep-ph/0302165.

- [26] G. Denicol, A. Monnai, B. Schenke, Moving forward to constrain the shear viscosity of QCD matter, arXiv:1512.01538 [nucl-th].
- [27] E. Molnar, H. Holopainen, P. Huovinen, H. Niemi, Influence of temperature dependent shear viscosity on elliptic flow at back- and forward rapidities in ultra-relativistic heavy-ion collisions, Phys. Rev. C 90 (2014) 044904, arXiv:1407.8152 [nucl-th].
- [28] F.G. Gardim, F. Grassi, M. Luzum, J.-Y. Ollitrault, Breaking of factorization of two-particle correlations in hydrodynamics, Phys. Rev. C 87 (3) (2013) 031901, arXiv:1211.0989 [nucl-th].
- [29] J. Jia, P. Huo, A method for studying the rapidity fluctuation and decorrelation of harmonic flow in heavy-ion collisions, Phys. Rev. C 90 (2014) 034905, arXiv:1402.6680 [nucl-th].
- [30] CMS Collaboration, V. Khachatryan, et al., Evidence for transverse momentum and pseudorapidity dependent event plane fluctuations in PbPb and pPb collisions, Phys. Rev. C 92 (3) (2015) 034911, arXiv:1503.01692 [nucl-ex].
- [31] PHOBOS Collaboration, B. Back, et al., Pseudorapidity and centrality dependence of the collective flow of charged particles in Au + Au collisions at $\sqrt{s_{NN}} = 130$ GeV, Phys. Rev. Lett. 89 (2002) 222301, arXiv:nucl-ex/0205021.
- [32] PHOBOS Collaboration, B. Back, et al., Centrality and pseudorapidity dependence of elliptic flow for charged hadrons in Au + Au collisions at 200 GeV, Phys. Rev. C 72 (2005) 051901, arXiv:nucl-ex/0407012.
- [33] PHOBOS Collaboration, B. Back, et al., Energy dependence of elliptic flow over a large pseudorapidity range in Au + Au collisions at RHIC, Phys. Rev. Lett. 94 (2005) 122303, arXiv:nucl-ex/0406021.
- [34] PHOBOS Collaboration, B. Alver, et al., System size, energy, pseudorapidity, and centrality dependence of elliptic flow, Phys. Rev. Lett. 98 (2007) 242302, arXiv:nucl-ex/0610037.
- [35] BRAHMS Collaboration, I. Bearden, et al., Pseudorapidity distributions of charged particles from Au + Au collisions at the maximum RHIC energy, Phys. Rev. Lett. 88 (2002) 202301, arXiv:nucl-ex/0112001.
- [36] PHOBOS Collaboration, B. Alver, et al., Phobos results on charged particle multiplicity and pseudorapidity distributions in Au + Au, Cu + Cu, d + Au, and p + p collisions at ultra-relativistic energies, Phys. Rev. C 83 (2011) 024913, arXiv:1011.1940 [nucl-ex].
- [37] PHOBOS Collaboration, B. Back, et al., Energy dependence of directed flow over a wide range of pseudorapidity in Au + Au collisions at RHIC, Phys. Rev. Lett. 97 (2006) 012301, arXiv:nucl-ex/0511045.
- [38] ATLAS Collaboration, G. Aad, et al., Measurement of the centrality and pseudorapidity dependence of the integrated elliptic flow in lead-lead collisions at $\sqrt{s_{NN}} = 2.76$ TeV with the ATLAS detector, Eur. Phys. J. C 74 (8) (2014) 2982, arXiv:1405.3936 [hep-ex].
- [39] ALICE Collaboration, E. Abbas, et al., Centrality dependence of the pseudorapidity density distribution for charged particles in Pb-Pb collisions at $\sqrt{s_{NN}} = 2.76$ TeV, Phys. Lett. B 726 (2013) 610–622, arXiv:1304.0347 [nucl-ex].
- [40] ALICE Collaboration, K. Aamodt, et al., The ALICE experiment at the CERN LHC, J. Instrum. 3 (2008), S08002.
- [41] ALICE Collaboration, E. Abbas, et al., Performance of the ALICE VZERO system, J. Instrum. 8 (2013) P10016, arXiv:1306.3130 [nucl-ex].
- [42] J. Alme, Y. Andres, H. Appelshäuser, S. Bablok, N. Bialas, et al., The ALICE TPC, a large 3-dimensional tracking device with fast readout for ultra-high multiplicity events, Nucl. Instrum. Methods Phys. Res., Sect. A, Accel. Spectrom. Detect. Assoc. Equip. 622 (2010) 316–367, arXiv:1001.1950 [physics.ins-det].
- [43] C.H. Christensen, J.J. Gaardhoje, K. Gulbrandsen, B.S. Nielsen, C. Sogaard, The ALICE forward multiplicity detector, Int. J. Mod. Phys. E 16 (2007) 2432–2437, arXiv:0712.1117 [nucl-ex].
- [44] ALICE Collaboration, B. Abelev, et al., Centrality determination of Pb-Pb collisions at $\sqrt{s_{NN}} = 2.76$ TeV with ALICE, Phys. Rev. C 88 (4) (2013) 044909, arXiv:1301.4361 [nucl-ex].
- [45] A. Bilandzic, R. Snellings, S. Voloshin, Flow analysis with cumulants: direct calculations, Phys. Rev. C 83 (2011) 044913, arXiv:1010.0233 [nucl-ex].
- [46] A. Hansen, Pseudorapidity dependence of anisotropic azimuthal flow with the ALICE detector, <http://www.nbi.dk/~alex/pdf/thesis.pdf>, 2014, Ph.D. thesis.
- [47] A. Bilandzic, C.H. Christensen, K. Gulbrandsen, A. Hansen, Y. Zhou, Generic framework for anisotropic flow analyses with multi-particle azimuthal correlations, Phys. Rev. C 89 (2014) 064904, arXiv:1312.3572 [nucl-ex].
- [48] R. Brun, F. Carminati, S. Giani, GEANT detector description and simulation tool, <http://wwwinfo.cern.ch/asdoc/psdir/geant/geantall.ps.gz>, 1994.
- [49] Z.-W. Lin, C.M. Ko, B.-A. Li, B. Zhang, S. Pal, A multi-phase transport model for relativistic heavy ion collisions, Phys. Rev. C 72 (2005) 064901, arXiv:nucl-th/0411110.
- [50] J. Xu, C.M. Ko, Pb-Pb collisions at $\sqrt{s_{NN}} = 2.76$ TeV in a multiphase transport model, Phys. Rev. C 83 (2011) 034904, arXiv:1101.2231 [nucl-th].
- [51] ALICE Collaboration, B.B. Abelev, et al., Multi-particle azimuthal correlations in p-Pb and Pb-Pb collisions at the CERN large hadron collider, Phys. Rev. C 90 (5) (2014) 054901, arXiv:1406.2474 [nucl-ex].
- [52] X.-N. Wang, M. Gyulassy, HIJING: a Monte Carlo model for multiple jet production in p p, p A and A A collisions, Phys. Rev. D 44 (1991) 3501–3516.
- [53] S.A. Voloshin, A.M. Poskanzer, R. Snellings, Collective phenomena in non-central nuclear collisions, arXiv:0809.2949 [nucl-ex].

ALICE Collaboration

J. Adam ³⁹, D. Adamová ⁸⁵, M.M. Aggarwal ⁸⁹, G. Aglieri Rinella ³⁵, M. Agnello ¹¹¹, N. Agrawal ⁴⁸, Z. Ahammed ¹³⁴, S. Ahmad ¹⁹, S.U. Ahn ⁶⁹, S. Aiola ¹³⁸, A. Akindinov ⁵⁹, S.N. Alam ¹³⁴, D.S.D. Albuquerque ¹²², D. Aleksandrov ⁸¹, B. Alessandro ¹¹¹, D. Alexandre ¹⁰², R. Alfaro Molina ⁶⁵, A. Alici ^{12,105}, A. Alkin ³, J.R.M. Almaraz ¹²⁰, J. Alme ^{18,37}, T. Alt ⁴², S. Altinpinar ¹⁸, I. Altsybeev ¹³³, C. Alves Garcia Prado ¹²¹, C. Andrei ⁷⁹, A. Andronic ⁹⁸, V. Anguelov ⁹⁵, T. Antićić ⁹⁹, F. Antinori ¹⁰⁸, P. Antonioli ¹⁰⁵, L. Aphecetche ¹¹⁴, H. Appelshäuser ⁵⁴, S. Arcelli ²⁷, R. Arnaldi ¹¹¹, O.W. Arnold ^{94,36}, I.C. Arsene ²², M. Arslanbekov ⁵⁴, B. Audurier ¹¹⁴, A. Augustinus ³⁵, R. Averbeck ⁹⁸, M.D. Azmi ¹⁹, A. Badalà ¹⁰⁷, Y.W. Baek ⁶⁸, S. Bagnasco ¹¹¹, R. Bailhache ⁵⁴, R. Bala ⁹², S. Balasubramanian ¹³⁸, A. Baldissari ¹⁵, R.C. Baral ⁶², A.M. Barbano ²⁶, R. Barbera ²⁸, F. Barile ³², G.G. Barnaföldi ¹³⁷, L.S. Barnby ^{102,35}, V. Barret ⁷¹, P. Bartalini ⁷, K. Barth ³⁵, J. Bartke ^{118,i}, E. Bartsch ⁵⁴, M. Basile ²⁷, N. Bastid ⁷¹, S. Basu ¹³⁴, B. Bathen ⁵⁵, G. Batigne ¹¹⁴, A. Batista Camejo ⁷¹, B. Batyunya ⁶⁷, P.C. Bätzing ²², I.G. Bearden ⁸², H. Beck ^{54,95}, C. Bedda ¹¹¹, N.K. Behera ^{49,51}, I. Belikov ⁵⁶, F. Bellini ²⁷, H. Bello Martinez ², R. Bellwied ¹²³, R. Belmont ¹³⁶, E. Belmont-Moreno ⁶⁵, L.G.E. Beltran ¹²⁰, V. Belyaev ⁷⁶, G. Bencedi ¹³⁷, S. Beole ²⁶, I. Berceanu ⁷⁹, A. Bercuci ⁷⁹, Y. Berdnikov ⁸⁷, D. Berenyi ¹³⁷, R.A. Bertens ⁵⁸, D. Berziano ³⁵, L. Betev ³⁵, A. Bhasin ⁹², I.R. Bhat ⁹², A.K. Bhati ⁸⁹, B. Bhattacharjee ⁴⁴, J. Bhom ^{129,118}, L. Bianchi ¹²³, N. Bianchi ⁷³, C. Bianchin ¹³⁶, J. Bielčík ³⁹, J. Bielčíková ⁸⁵, A. Bilandzic ^{82,36,94}, G. Biro ¹³⁷, R. Biswas ⁴, S. Biswas ^{4,80}, S. Bjelogrlic ⁵⁸, J.T. Blair ¹¹⁹, D. Blau ⁸¹, C. Blume ⁵⁴, F. Bock ^{75,95}, A. Bogdanov ⁷⁶, H. Bøggild ⁸², L. Boldizsár ¹³⁷, M. Bombara ⁴⁰, M. Bonora ³⁵, J. Book ⁵⁴, H. Borel ¹⁵, A. Borissov ⁹⁷, M. Borri ^{84,125}, F. Bossú ⁶⁶, E. Botta ²⁶, C. Bourjau ⁸², P. Braun-Munzinger ⁹⁸, M. Bregant ¹²¹, T. Breitner ⁵³, T.A. Broker ⁵⁴, T.A. Browning ⁹⁶, M. Broz ³⁹, E.J. Brucken ⁴⁶, E. Bruna ¹¹¹, G.E. Bruno ³², D. Budnikov ¹⁰⁰, H. Buesching ⁵⁴, S. Bufalino ^{35,26}, P. Buncic ³⁵, O. Busch ¹²⁹, Z. Buthelezi ⁶⁶, J.B. Butt ¹⁶, J.T. Buxton ²⁰, J. Cabala ¹¹⁶, D. Caffarri ³⁵, X. Cai ⁷, H. Caines ¹³⁸, L. Calero Diaz ⁷³, A. Caliva ⁵⁸, E. Calvo Villar ¹⁰³, P. Camerini ²⁵, F. Carena ³⁵, W. Carena ³⁵, F. Carnesecchi ²⁷, J. Castillo Castellanos ¹⁵, A.J. Castro ¹²⁶,

- E.A.R. Casula ²⁴, C. Ceballos Sanchez ⁹, J. Cepila ³⁹, P. Cerello ¹¹¹, J. Cerkala ¹¹⁶, B. Chang ¹²⁴,
 S. Chapeland ³⁵, M. Chartier ¹²⁵, J.L. Charvet ¹⁵, S. Chattopadhyay ¹³⁴, S. Chattopadhyay ¹⁰¹,
 A. Chauvin ^{94,36}, V. Chelnokov ³, M. Cherney ⁸⁸, C. Cheshkov ¹³¹, B. Cheynis ¹³¹, V. Chibante Barroso ³⁵,
 D.D. Chinellato ¹²², S. Cho ⁵¹, P. Chochula ³⁵, K. Choi ⁹⁷, M. Chojnacki ⁸², S. Choudhury ¹³⁴,
 P. Christakoglou ⁸³, C.H. Christensen ⁸², P. Christiansen ³³, T. Chujo ¹²⁹, S.U. Chung ⁹⁷, C. Cicalo ¹⁰⁶,
 L. Cifarelli ^{12,27}, F. Cindolo ¹⁰⁵, J. Cleymans ⁹¹, F. Colamaria ³², D. Colella ^{60,35}, A. Collu ⁷⁵, M. Colocci ²⁷,
 G. Conesa Balbastre ⁷², Z. Conesa del Valle ⁵², M.E. Connors ^{138,ii}, J.G. Contreras ³⁹, T.M. Cormier ⁸⁶,
 Y. Corrales Morales ^{111,26}, I. Cortés Maldonado ², P. Cortese ³¹, M.R. Cosentino ¹²¹, F. Costa ³⁵,
 J. Crkovska ⁵², P. Crochet ⁷¹, R. Cruz Albino ¹¹, E. Cuautle ⁶⁴, L. Cunqueiro ^{55,35}, T. Dahms ^{94,36},
 A. Dainese ¹⁰⁸, M.C. Danisch ⁹⁵, A. Danu ⁶³, D. Das ¹⁰¹, I. Das ¹⁰¹, S. Das ⁴, A. Dash ⁸⁰, S. Dash ⁴⁸, S. De ¹²¹,
 A. De Caro ^{12,30}, G. de Cataldo ¹⁰⁴, C. de Conti ¹²¹, J. de Cuveland ⁴², A. De Falco ²⁴, D. De Gruttola ^{12,30},
 N. De Marco ¹¹¹, S. De Pasquale ³⁰, R.D. De Souza ¹²², A. Deisting ^{95,98}, A. Deloff ⁷⁸, E. Dénes ^{137,i},
 C. Deplano ⁸³, P. Dhankher ⁴⁸, D. Di Bari ³², A. Di Mauro ³⁵, P. Di Nezza ⁷³, B. Di Ruzza ¹⁰⁸,
 M.A. Diaz Corchero ¹⁰, T. Dietel ⁹¹, P. Dillenseger ⁵⁴, R. Divià ³⁵, Ø. Djupsland ¹⁸, A. Dobrin ^{83,63},
 D. Domenicis Gimenez ¹²¹, B. Dönigus ⁵⁴, O. Dordic ²², T. Drozhzhova ⁵⁴, A.K. Dubey ¹³⁴, A. Dubla ⁵⁸,
 L. Ducroux ¹³¹, P. Dupieux ⁷¹, R.J. Ehlers ¹³⁸, D. Elia ¹⁰⁴, E. Endress ¹⁰³, H. Engel ⁵³, E. Epple ¹³⁸,
 B. Erazmus ¹¹⁴, I. Erdemir ⁵⁴, F. Erhardt ¹³⁰, B. Espagnon ⁵², M. Estienne ¹¹⁴, S. Esumi ¹²⁹, J. Eum ⁹⁷,
 D. Evans ¹⁰², S. Evdokimov ¹¹², G. Eyyubova ³⁹, L. Fabbietti ^{94,36}, D. Fabris ¹⁰⁸, J. Faivre ⁷², A. Fantoni ⁷³,
 M. Fasel ⁷⁵, L. Feldkamp ⁵⁵, A. Feliciello ¹¹¹, G. Feofilov ¹³³, J. Ferencei ⁸⁵, A. Fernández Téllez ²,
 E.G. Ferreiro ¹⁷, A. Ferretti ²⁶, A. Festanti ²⁹, V.J.G. Feuillard ^{15,71}, J. Figiel ¹¹⁸, M.A.S. Figueiredo ^{125,121},
 S. Filchagin ¹⁰⁰, D. Finogeev ⁵⁷, F.M. Fionda ²⁴, E.M. Fiore ³², M.G. Fleck ⁹⁵, M. Floris ³⁵, S. Foertsch ⁶⁶,
 P. Foka ⁹⁸, S. Fokin ⁸¹, E. Fragiocomo ¹¹⁰, A. Francescon ³⁵, A. Francisco ¹¹⁴, U. Frankenfeld ⁹⁸,
 G.G. Fronze ²⁶, U. Fuchs ³⁵, C. Furget ⁷², A. Furs ⁵⁷, M. Fusco Girard ³⁰, J.J. Gaardhøje ⁸², M. Gagliardi ²⁶,
 A.M. Gago ¹⁰³, K. Gajdosova ⁸², M. Gallio ²⁶, C.D. Galvan ¹²⁰, D.R. Gangadharan ⁷⁵, P. Ganoti ⁹⁰, C. Gao ⁷,
 C. Garabatos ⁹⁸, E. Garcia-Solis ¹³, C. Gargiulo ³⁵, P. Gasik ^{94,36}, E.F. Gauger ¹¹⁹, M. Germain ¹¹⁴,
 M. Gheata ^{35,63}, P. Ghosh ¹³⁴, S.K. Ghosh ⁴, P. Gianotti ⁷³, P. Giubellino ^{111,35}, P. Giubilato ²⁹,
 E. Gladysz-Dziadus ¹¹⁸, P. Glässel ⁹⁵, D.M. Goméz Coral ⁶⁵, A. Gomez Ramirez ⁵³, A.S. Gonzalez ³⁵,
 V. Gonzalez ¹⁰, P. González-Zamora ¹⁰, S. Gorbunov ⁴², L. Görlich ¹¹⁸, S. Gotovac ¹¹⁷, V. Grabski ⁶⁵,
 O.A. Grachov ¹³⁸, L.K. Graczykowski ¹³⁵, K.L. Graham ¹⁰², A. Grelli ⁵⁸, A. Grigoras ³⁵, C. Grigoras ³⁵,
 V. Grigoriev ⁷⁶, A. Grigoryan ¹, S. Grigoryan ⁶⁷, B. Grinyov ³, N. Grion ¹¹⁰, J.M. Gronefeld ⁹⁸,
 J.F. Grosse-Oetringhaus ³⁵, R. Grossi ⁹⁸, L. Gruber ¹¹³, F. Guber ⁵⁷, R. Guernane ⁷², B. Guerzoni ²⁷,
 K. Gulbrandsen ⁸², T. Gunji ¹²⁸, A. Gupta ⁹², R. Gupta ⁹², R. Haake ³⁵, Ø. Haaland ¹⁸, C. Hadjidakis ⁵²,
 M. Haiduc ⁶³, H. Hamagaki ¹²⁸, G. Hamar ¹³⁷, J.C. Hamon ⁵⁶, A. Hansen ⁸², J.W. Harris ¹³⁸, A. Harton ¹³,
 D. Hatzifotiadou ¹⁰⁵, S. Hayashi ¹²⁸, S.T. Heckel ⁵⁴, E. Hellbär ⁵⁴, H. Helstrup ³⁷, A. Hergheliegiu ⁷⁹,
 G. Herrera Corral ¹¹, B.A. Hess ³⁴, K.F. Hetland ³⁷, H. Hillemanns ³⁵, B. Hippolyte ⁵⁶, D. Horak ³⁹,
 R. Hosokawa ¹²⁹, P. Hristov ³⁵, C. Hughes ¹²⁶, T.J. Humanic ²⁰, N. Hussain ⁴⁴, T. Hussain ¹⁹, D. Hutter ⁴²,
 D.S. Hwang ²¹, R. Ilkaev ¹⁰⁰, M. Inaba ¹²⁹, E. Incani ²⁴, M. Ippolitov ^{76,81}, M. Irfan ¹⁹, M. Ivanov ⁹⁸,
 V. Ivanov ⁸⁷, V. Izucheev ¹¹², B. Jacak ⁷⁵, N. Jacazio ²⁷, P.M. Jacobs ⁷⁵, M.B. Jadhav ⁴⁸, S. Jadlovska ¹¹⁶,
 J. Jadlovsky ^{116,60}, C. Jahnke ¹²¹, M.J. Jakubowska ¹³⁵, H.J. Jang ⁶⁹, M.A. Janik ¹³⁵, P.H.S.Y. Jayarathna ¹²³,
 C. Jena ²⁹, S. Jena ¹²³, R.T. Jimenez Bustamante ⁹⁸, P.G. Jones ¹⁰², A. Jusko ¹⁰², P. Kalinak ⁶⁰, A. Kalweit ³⁵,
 J.H. Kang ¹³⁹, V. Kaplin ⁷⁶, S. Kar ¹³⁴, A. Karasu Uysal ⁷⁰, O. Karavichev ⁵⁷, T. Karavicheva ⁵⁷,
 L. Karayan ^{98,95}, E. Karpechev ⁵⁷, U. Kebschull ⁵³, R. Keidel ¹⁴⁰, D.L.D. Keijdener ⁵⁸, M. Keil ³⁵,
 M. Mohisin Khan ^{19,iii}, P. Khan ¹⁰¹, S.A. Khan ¹³⁴, A. Khanzadeev ⁸⁷, Y. Kharlov ¹¹², B. Kileng ³⁷,
 D.W. Kim ⁴³, D.J. Kim ¹²⁴, D. Kim ¹³⁹, H. Kim ¹³⁹, J.S. Kim ⁴³, J. Kim ⁹⁵, M. Kim ¹³⁹, S. Kim ²¹, T. Kim ¹³⁹,
 S. Kirsch ⁴², I. Kisiel ⁴², S. Kiselev ⁵⁹, A. Kisiel ¹³⁵, G. Kiss ¹³⁷, J.L. Klay ⁶, C. Klein ⁵⁴, J. Klein ³⁵,
 C. Klein-Bösing ⁵⁵, S. Klewin ⁹⁵, A. Kluge ³⁵, M.L. Knichel ⁹⁵, A.G. Knospe ^{119,123}, C. Kobdaj ¹¹⁵,
 M. Kofarago ³⁵, T. Kollegger ⁹⁸, A. Kolojvari ¹³³, V. Kondratiev ¹³³, N. Kondratyeva ⁷⁶, E. Kondratyuk ¹¹²,
 A. Konevskikh ⁵⁷, M. Kopcik ¹¹⁶, M. Kour ⁹², C. Kouzinopoulos ³⁵, O. Kovalenko ⁷⁸, V. Kovalenko ¹³³,
 M. Kowalski ¹¹⁸, G. Koyithatta Meethaleveedu ⁴⁸, I. Králik ⁶⁰, A. Kravčáková ⁴⁰, M. Krivda ^{60,102},
 F. Krizek ⁸⁵, E. Kryshen ^{87,35}, M. Krzewicki ⁴², A.M. Kubera ²⁰, V. Kučera ⁸⁵, C. Kuhn ⁵⁶, P.G. Kuijer ⁸³,
 A. Kumar ⁹², J. Kumar ⁴⁸, L. Kumar ⁸⁹, S. Kumar ⁴⁸, P. Kurashvili ⁷⁸, A. Kurepin ⁵⁷, A.B. Kurepin ⁵⁷,
 A. Kuryakin ¹⁰⁰, M.J. Kweon ⁵¹, Y. Kwon ¹³⁹, S.L. La Pointe ¹¹¹, P. La Rocca ²⁸, P. Ladron de Guevara ¹¹,

- C. Lagana Fernandes ¹²¹, I. Lakomov ³⁵, R. Langoy ⁴¹, K. Lapidus ^{138,36}, C. Lara ⁵³, A. Lardeux ¹⁵,
 A. Lattuca ²⁶, E. Laudi ³⁵, R. Lea ²⁵, L. Leardini ⁹⁵, S. Lee ¹³⁹, F. Lehas ⁸³, S. Lehner ¹¹³, R.C. Lemmon ⁸⁴,
 V. Lenti ¹⁰⁴, E. Leogrande ⁵⁸, I. León Monzón ¹²⁰, H. León Vargas ⁶⁵, M. Leoncino ²⁶, P. Lévai ¹³⁷, S. Li ^{71,7},
 X. Li ¹⁴, J. Lien ⁴¹, R. Lietava ¹⁰², S. Lindal ²², V. Lindenstruth ⁴², C. Lippmann ⁹⁸, M.A. Lisa ²⁰,
 H.M. Ljunggren ³³, D.F. Lodato ⁵⁸, P.I. Loenne ¹⁸, V. Loginov ⁷⁶, C. Loizides ⁷⁵, X. Lopez ⁷¹, E. López Torres ⁹,
 A. Lowe ¹³⁷, P. Luettig ⁵⁴, M. Lunardon ²⁹, G. Luparello ²⁵, M. Lupi ³⁵, T.H. Lutz ¹³⁸, A. Maevskaya ⁵⁷,
 M. Mager ³⁵, S. Mahajan ⁹², S.M. Mahmood ²², A. Maire ⁵⁶, R.D. Majka ¹³⁸, M. Malaev ⁸⁷,
 I. Maldonado Cervantes ⁶⁴, L. Malinina ^{67,iv}, D. Mal'Kevich ⁵⁹, P. Malzacher ⁹⁸, A. Mamontov ¹⁰⁰,
 V. Manko ⁸¹, F. Manso ⁷¹, V. Manzari ^{35,104}, Y. Mao ⁷, M. Marchisone ^{127,66,26}, J. Mareš ⁶¹,
 G.V. Margagliotti ²⁵, A. Margotti ¹⁰⁵, J. Margutti ⁵⁸, A. Marín ⁹⁸, C. Markert ¹¹⁹, M. Marquard ⁵⁴,
 N.A. Martin ⁹⁸, J. Martin Blanco ¹¹⁴, P. Martinengo ³⁵, M.I. Martínez ², G. Martínez García ¹¹⁴,
 M. Martinez Pedreira ³⁵, A. Mas ¹²¹, S. Masciocchi ⁹⁸, M. Masera ²⁶, A. Masoni ¹⁰⁶, A. Mastrosorio ³²,
 A. Matyja ¹¹⁸, C. Mayer ¹¹⁸, J. Mazer ¹²⁶, M.A. Mazzoni ¹⁰⁹, D. McDonald ¹²³, F. Meddi ²³, Y. Melikyan ⁷⁶,
 A. Menchaca-Rocha ⁶⁵, E. Meninno ³⁰, J. Mercado Pérez ⁹⁵, M. Meres ³⁸, S. Mhlanga ⁹¹, Y. Miake ¹²⁹,
 M.M. Mieskolainen ⁴⁶, K. Mikhaylov ^{67,59}, L. Milano ^{75,35}, J. Milosevic ²², A. Mischke ⁵⁸, A.N. Mishra ⁴⁹,
 D. Miśkowiec ⁹⁸, J. Mitra ¹³⁴, C.M. Mitu ⁶³, N. Mohammadi ⁵⁸, B. Mohanty ⁸⁰, L. Molnar ⁵⁶,
 L. Montaño Zetina ¹¹, E. Montes ¹⁰, D.A. Moreira De Godoy ⁵⁵, L.A.P. Moreno ², S. Moretto ²⁹,
 A. Morreale ¹¹⁴, A. Morsch ³⁵, V. Muccifora ⁷³, E. Mudnic ¹¹⁷, D. Mühlheim ⁵⁵, S. Muhuri ¹³⁴,
 M. Mukherjee ¹³⁴, J.D. Mulligan ¹³⁸, M.G. Munhoz ¹²¹, K. Münning ⁴⁵, R.H. Munzer ^{36,54,94},
 H. Murakami ¹²⁸, S. Murray ⁶⁶, L. Musa ³⁵, J. Musinsky ⁶⁰, B. Naik ⁴⁸, R. Nair ⁷⁸, B.K. Nandi ⁴⁸, R. Nania ¹⁰⁵,
 E. Nappi ¹⁰⁴, M.U. Naru ¹⁶, H. Natal da Luz ¹²¹, C. Nattrass ¹²⁶, S.R. Navarro ², K. Nayak ⁸⁰, R. Nayak ⁴⁸,
 T.K. Nayak ¹³⁴, S. Nazarenko ¹⁰⁰, A. Nedosekin ⁵⁹, R.A. Negrao De Oliveira ³⁵, L. Nellen ⁶⁴, F. Ng ¹²³,
 M. Nicassio ⁹⁸, M. Niculescu ⁶³, J. Niedziela ³⁵, B.S. Nielsen ⁸², S. Nikolaev ⁸¹, S. Nikulin ⁸¹, V. Nikulin ⁸⁷,
 F. Noferini ^{105,12}, P. Nomokonov ⁶⁷, G. Nooren ⁵⁸, J.C.C. Noris ², J. Norman ¹²⁵, A. Nyanin ⁸¹, J. Nystrand ¹⁸,
 H. Oeschler ⁹⁵, S. Oh ¹³⁸, S.K. Oh ⁶⁸, A. Ohlson ³⁵, A. Okatan ⁷⁰, T. Okubo ⁴⁷, J. Oleniacz ¹³⁵,
 A.C. Oliveira Da Silva ¹²¹, M.H. Oliver ¹³⁸, J. Onderwaater ⁹⁸, C. Oppedisano ¹¹¹, R. Orava ⁴⁶, M. Oravec ¹¹⁶,
 A. Ortiz Velasquez ⁶⁴, A. Oskarsson ³³, J. Otwinowski ¹¹⁸, K. Oyama ^{95,77}, M. Ozdemir ⁵⁴, Y. Pachmayer ⁹⁵,
 D. Pagano ¹³², P. Pagano ³⁰, G. Paić ⁶⁴, S.K. Pal ¹³⁴, J. Pan ¹³⁶, A.K. Pandey ⁴⁸, V. Papikyan ¹,
 G.S. Pappalardo ¹⁰⁷, P. Pareek ⁴⁹, W.J. Park ⁹⁸, S. Parmar ⁸⁹, A. Passfeld ⁵⁵, V. Paticchio ¹⁰⁴, R.N. Patra ¹³⁴,
 B. Paul ^{111,101}, H. Pei ⁷, T. Peitzmann ⁵⁸, H. Pereira Da Costa ¹⁵, D. Peresunko ^{81,76}, E. Perez Lezama ⁵⁴,
 V. Peskov ⁵⁴, Y. Pestov ⁵, V. Petráček ³⁹, V. Petrov ¹¹², M. Petrovici ⁷⁹, C. Petta ²⁸, S. Piano ¹¹⁰, M. Pikna ³⁸,
 P. Pillot ¹¹⁴, L.O.D.L. Pimentel ⁸², O. Pinazza ^{105,35}, L. Pinsky ¹²³, D.B. Piyarathna ¹²³, M. Płoskoń ⁷⁵,
 M. Planinic ¹³⁰, J. Pluta ¹³⁵, S. Pochybova ¹³⁷, P.L.M. Podesta-Lerma ¹²⁰, M.G. Poghosyan ^{86,88},
 B. Polichtchouk ¹¹², N. Poljak ¹³⁰, W. Poonsawat ¹¹⁵, A. Pop ⁷⁹, H. Poppenborg ⁵⁵,
 S. Porteboeuf-Houssais ⁷¹, J. Porter ⁷⁵, J. Pospisil ⁸⁵, S.K. Prasad ⁴, R. Preghenella ^{105,35}, F. Prino ¹¹¹,
 C.A. Pruneau ¹³⁶, I. Pshenichnov ⁵⁷, M. Puccio ²⁶, G. Puddu ²⁴, P. Pujahari ¹³⁶, V. Punin ¹⁰⁰, J. Putschke ¹³⁶,
 H. Qvigstad ²², A. Rachevski ¹¹⁰, S. Raha ⁴, S. Rajput ⁹², J. Rak ¹²⁴, A. Rakotozafindrabe ¹⁵, L. Ramello ³¹,
 F. Rami ⁵⁶, R. Raniwala ⁹³, S. Raniwala ⁹³, S.S. Räsänen ⁴⁶, B.T. Rascanu ⁵⁴, D. Rathee ⁸⁹, K.F. Read ^{126,86},
 K. Redlich ⁷⁸, R.J. Reed ¹³⁶, A. Rehman ¹⁸, P. Reichelt ⁵⁴, F. Reidt ^{35,95}, X. Ren ⁷, R. Renfordt ⁵⁴,
 A.R. Reolon ⁷³, A. Reshetin ⁵⁷, K. Reygers ⁹⁵, V. Riabov ⁸⁷, R.A. Ricci ⁷⁴, T. Richert ³³, M. Richter ²²,
 P. Riedler ³⁵, W. Riegler ³⁵, F. Riggi ²⁸, C. Ristea ⁶³, E. Rocco ⁵⁸, M. Rodríguez Cahuantzi ²,
 A. Rodriguez Manso ⁸³, K. Røed ²², E. Rogochaya ⁶⁷, D. Rohr ⁴², D. Röhrich ¹⁸, F. Ronchetti ^{73,35},
 L. Ronflette ¹¹⁴, P. Rosnet ⁷¹, A. Rossi ²⁹, F. Roukoutakis ⁹⁰, A. Roy ⁴⁹, C. Roy ⁵⁶, P. Roy ¹⁰¹,
 A.J. Rubio Montero ¹⁰, R. Rui ²⁵, R. Russo ²⁶, E. Ryabinkin ⁸¹, Y. Ryabov ⁸⁷, A. Rybicki ¹¹⁸, S. Saarinen ⁴⁶,
 S. Sadhu ¹³⁴, S. Sadovsky ¹¹², K. Šafařík ³⁵, B. Sahlmuller ⁵⁴, P. Sahoo ⁴⁹, R. Sahoo ⁴⁹, S. Sahoo ⁶²,
 P.K. Sahu ⁶², J. Saini ¹³⁴, S. Sakai ⁷³, M.A. Saleh ¹³⁶, J. Salzwedel ²⁰, S. Sambyal ⁹², V. Samsonov ^{76,87},
 L. Šándor ⁶⁰, A. Sandoval ⁶⁵, M. Sano ¹²⁹, D. Sarkar ¹³⁴, N. Sarkar ¹³⁴, P. Sarma ⁴⁴, E. Scapparone ¹⁰⁵,
 F. Scarlassara ²⁹, C. Schiaua ⁷⁹, R. Schicker ⁹⁵, C. Schmidt ⁹⁸, H.R. Schmidt ³⁴, M. Schmidt ³⁴,
 S. Schuchmann ^{54,95}, J. Schukraft ³⁵, Y. Schultz ^{35,114}, K. Schwarz ⁹⁸, K. Schweda ⁹⁸, G. Scioli ²⁷,
 E. Scomparin ¹¹¹, R. Scott ¹²⁶, M. Šefčík ⁴⁰, J.E. Seger ⁸⁸, Y. Sekiguchi ¹²⁸, D. Sekihata ⁴⁷, I. Selyuzhenkov ⁹⁸,
 K. Senosi ⁶⁶, S. Senyukov ^{3,35}, E. Serradilla ^{10,65}, A. Sevcenco ⁶³, A. Shabanov ⁵⁷, A. Shabetai ¹¹⁴,
 O. Shadura ³, R. Shahoyan ³⁵, M.I. Shahzad ¹⁶, A. Shangaraev ¹¹², A. Sharma ⁹², M. Sharma ⁹²,

M. Sharma ⁹², N. Sharma ¹²⁶, A.I. Sheikh ¹³⁴, K. Shigaki ⁴⁷, Q. Shou ⁷, K. Shtejer ^{9,26}, Y. Sibiriak ⁸¹,
 S. Siddhanta ¹⁰⁶, K.M. Sielewicz ³⁵, T. Siemianczuk ⁷⁸, D. Silvermyr ³³, C. Silvestre ⁷², G. Simatovic ¹³⁰,
 G. Simonetti ³⁵, R. Singaraju ¹³⁴, R. Singh ⁸⁰, V. Singhal ¹³⁴, T. Sinha ¹⁰¹, B. Sitar ³⁸, M. Sitta ³¹,
 T.B. Skaali ²², M. Slupecki ¹²⁴, N. Smirnov ¹³⁸, R.J.M. Snellings ⁵⁸, T.W. Snellman ¹²⁴, J. Song ⁹⁷, M. Song ¹³⁹,
 Z. Song ⁷, F. Soramel ²⁹, S. Sorensen ¹²⁶, F. Sozzi ⁹⁸, E. Spiriti ⁷³, I. Sputowska ¹¹⁸,
 M. Spyropoulou-Stassinaki ⁹⁰, J. Stachel ⁹⁵, I. Stan ⁶³, P. Stankus ⁸⁶, E. Stenlund ³³, G. Steyn ⁶⁶,
 J.H. Stiller ⁹⁵, D. Stocco ¹¹⁴, P. Strmen ³⁸, A.A.P. Suade ¹²¹, T. Sugitate ⁴⁷, C. Suire ⁵², M. Suleymanov ¹⁶,
 M. Suljic ^{25,i}, R. Sultanov ⁵⁹, M. Šumbera ⁸⁵, S. Sumowidagdo ⁵⁰, A. Szabo ³⁸, I. Szarka ³⁸,
 A. Szczepankiewicz ¹³⁵, M. Szymanski ¹³⁵, U. Tabassam ¹⁶, J. Takahashi ¹²², G.J. Tambave ¹⁸, N. Tanaka ¹²⁹,
 M. Tarhini ⁵², M. Tariq ¹⁹, M.G. Tarzila ⁷⁹, A. Tauro ³⁵, G. Tejeda Muñoz ², A. Telesca ³⁵, K. Terasaki ¹²⁸,
 C. Terrevoli ²⁹, B. Teyssier ¹³¹, J. Thäder ⁷⁵, D. Thakur ⁴⁹, D. Thomas ¹¹⁹, R. Tieulent ¹³¹, A. Tikhonov ⁵⁷,
 A.R. Timmins ¹²³, A. Toia ⁵⁴, S. Trogolo ²⁶, G. Trombetta ³², V. Trubnikov ³, W.H. Trzaska ¹²⁴, T. Tsuji ¹²⁸,
 A. Tumkin ¹⁰⁰, R. Turrisi ¹⁰⁸, T.S. Tveter ²², K. Ullaland ¹⁸, A. Uras ¹³¹, G.L. Usai ²⁴, A. Utrobiticic ¹³⁰,
 M. Vala ⁶⁰, L. Valencia Palomo ⁷¹, S. Vallero ²⁶, J. Van Der Maarel ⁵⁸, J.W. Van Hoorn ^{35,113},
 M. van Leeuwen ⁵⁸, T. Vanat ⁸⁵, P. Vande Vyvre ³⁵, D. Varga ¹³⁷, A. Vargas ², M. Vargyas ¹²⁴, R. Varma ⁴⁸,
 M. Vasileiou ⁹⁰, A. Vasiliev ⁸¹, A. Vauthier ⁷², O. Vázquez Doce ^{94,36}, V. Vechernin ¹³³, A.M. Veen ⁵⁸,
 M. Veldhoen ⁵⁸, A. Velure ¹⁸, E. Vercellin ²⁶, S. Vergara Limón ², R. Vernet ⁸, M. Verweij ¹³⁶, L. Vickovic ¹¹⁷,
 J. Viinikainen ¹²⁴, Z. Vilakazi ¹²⁷, O. Villalobos Baillie ¹⁰², A. Villatoro Tello ², A. Vinogradov ⁸¹,
 L. Vinogradov ¹³³, T. Virgili ³⁰, V. Vislavicius ³³, Y.P. Viyogi ¹³⁴, A. Vodopyanov ⁶⁷, M.A. Völk ⁹⁵,
 K. Voloshin ⁵⁹, S.A. Voloshin ¹³⁶, G. Volpe ^{32,137}, B. von Haller ³⁵, I. Vorobyev ^{94,36}, D. Vranic ^{98,35},
 J. Vrláková ⁴⁰, B. Vulpescu ⁷¹, B. Wagner ¹⁸, J. Wagner ⁹⁸, H. Wang ⁵⁸, M. Wang ⁷, D. Watanabe ¹²⁹,
 Y. Watanabe ¹²⁸, M. Weber ^{35,113}, S.G. Weber ⁹⁸, D.F. Weiser ⁹⁵, J.P. Wessels ⁵⁵, U. Westerhoff ⁵⁵,
 A.M. Whitehead ⁹¹, J. Wiechula ³⁴, J. Wikne ²², G. Wilk ⁷⁸, J. Wilkinson ⁹⁵, G.A. Willems ⁵⁵,
 M.C.S. Williams ¹⁰⁵, B. Windelband ⁹⁵, M. Winn ⁹⁵, P. Yang ⁷, S. Yano ⁴⁷, Z. Yasin ¹⁶, Z. Yin ⁷,
 H. Yokoyama ¹²⁹, I.-K. Yoo ⁹⁷, J.H. Yoon ⁵¹, V. Yurchenko ³, A. Zaborowska ¹³⁵, V. Zaccolo ⁸², A. Zaman ¹⁶,
 C. Zampolli ^{105,35}, H.J.C. Zanolli ¹²¹, S. Zaporozhets ⁶⁷, N. Zardoshti ¹⁰², A. Zarochentsev ¹³³, P. Závada ⁶¹,
 N. Zaviyalov ¹⁰⁰, H. Zbroszczyk ¹³⁵, I.S. Zgura ⁶³, M. Zhalov ⁸⁷, H. Zhang ^{18,7}, X. Zhang ^{75,7}, Y. Zhang ⁷,
 C. Zhang ⁵⁸, Z. Zhang ⁷, C. Zhao ²², N. Zhigareva ⁵⁹, D. Zhou ⁷, Y. Zhou ⁸², Z. Zhou ¹⁸, H. Zhu ^{7,18},
 J. Zhu ^{7,114}, A. Zichichi ^{27,12}, A. Zimmermann ⁹⁵, M.B. Zimmermann ^{55,35}, G. Zinovjev ³, M. Zyzak ⁴²

¹ A.I. Alikhanyan National Science Laboratory (Yerevan Physics Institute) Foundation, Yerevan, Armenia² Benemérita Universidad Autónoma de Puebla, Puebla, Mexico³ Bogolyubov Institute for Theoretical Physics, Kiev, Ukraine⁴ Bose Institute, Department of Physics and Centre for Astroparticle Physics and Space Science (CAPSS), Kolkata, India⁵ Budker Institute for Nuclear Physics, Novosibirsk, Russia⁶ California Polytechnic State University, San Luis Obispo, CA, United States⁷ Central China Normal University, Wuhan, China⁸ Centre de Calcul de l'IN2P3, Villeurbanne, France⁹ Centro de Aplicaciones Tecnológicas y Desarrollo Nuclear (CEADEN), Havana, Cuba¹⁰ Centro de Investigaciones Energéticas Medioambientales y Tecnológicas (CIEMAT), Madrid, Spain¹¹ Centro de Investigación y de Estudios Avanzados (CINVESTAV), Mexico City and Mérida, Mexico¹² Centro Fermi – Museo Storico della Fisica e Centro Studi e Ricerche "Enrico Fermi", Rome, Italy¹³ Chicago State University, Chicago, IL, United States¹⁴ China Institute of Atomic Energy, Beijing, China¹⁵ Commissariat à l'Energie Atomique, IRFU, Saclay, France¹⁶ COMSATS Institute of Information Technology (CIIT), Islamabad, Pakistan¹⁷ Departamento de Física de Partículas and ICFAE, Universidad de Santiago de Compostela, Santiago de Compostela, Spain¹⁸ Department of Physics and Technology, University of Bergen, Bergen, Norway¹⁹ Department of Physics, Aligarh Muslim University, Aligarh, India²⁰ Department of Physics, Ohio State University, Columbus, OH, United States²¹ Department of Physics, Sejong University, Seoul, South Korea²² Department of Physics, University of Oslo, Oslo, Norway²³ Dipartimento di Fisica dell'Università 'La Sapienza' and Sezione INFN, Rome, Italy²⁴ Dipartimento di Fisica dell'Università and Sezione INFN, Cagliari, Italy²⁵ Dipartimento di Fisica dell'Università and Sezione INFN, Trieste, Italy²⁶ Dipartimento di Fisica dell'Università and Sezione INFN, Turin, Italy²⁷ Dipartimento di Fisica e Astronomia dell'Università and Sezione INFN, Bologna, Italy²⁸ Dipartimento di Fisica e Astronomia dell'Università and Sezione INFN, Catania, Italy²⁹ Dipartimento di Fisica e Astronomia dell'Università and Sezione INFN, Padova, Italy³⁰ Dipartimento di Fisica 'E.R. Caianiello' dell'Università and Gruppo Collegato INFN, Salerno, Italy³¹ Dipartimento di Scienze e Innovazione Tecnologica dell'Università del Piemonte Orientale and Gruppo Collegato INFN, Alessandria, Italy³² Dipartimento Interateneo di Fisica 'M. Merlin' and Sezione INFN, Bari, Italy³³ Division of Experimental High Energy Physics, University of Lund, Lund, Sweden³⁴ Eberhard Karls Universität Tübingen, Tübingen, Germany

- ³⁵ European Organization for Nuclear Research (CERN), Geneva, Switzerland
³⁶ Excellence Cluster Universe, Technische Universität München, Munich, Germany
³⁷ Faculty of Engineering, Bergen University College, Bergen, Norway
³⁸ Faculty of Mathematics, Physics and Informatics, Comenius University, Bratislava, Slovakia
³⁹ Faculty of Nuclear Sciences and Physical Engineering, Czech Technical University in Prague, Prague, Czech Republic
⁴⁰ Faculty of Science, P.J. Šafárik University, Košice, Slovakia
⁴¹ Faculty of Technology, Buskerud and Vestfold University College, Vestfold, Norway
⁴² Frankfurt Institute for Advanced Studies, Johann Wolfgang Goethe-Universität Frankfurt, Frankfurt, Germany
⁴³ Gangneung-Wonju National University, Gangneung, South Korea
⁴⁴ Gauhati University, Department of Physics, Guwahati, India
⁴⁵ Helmholtz-Institut für Strahlen- und Kernphysik, Rheinische Friedrich-Wilhelms-Universität Bonn, Bonn, Germany
⁴⁶ Helsinki Institute of Physics (HIP), Helsinki, Finland
⁴⁷ Hiroshima University, Hiroshima, Japan
⁴⁸ Indian Institute of Technology Bombay (IIT), Mumbai, India
⁴⁹ Indian Institute of Technology Indore, Indore (IITI), India
⁵⁰ Indonesian Institute of Sciences, Jakarta, Indonesia
⁵¹ Inha University, Incheon, South Korea
⁵² Institut de Physique Nucléaire d'Orsay (IPNO), Université Paris-Sud, CNRS-IN2P3, Orsay, France
⁵³ Institut für Informatik, Johann Wolfgang Goethe-Universität Frankfurt, Frankfurt, Germany
⁵⁴ Institut für Kernphysik, Johann Wolfgang Goethe-Universität Frankfurt, Frankfurt, Germany
⁵⁵ Institut für Kernphysik, Westfälische Wilhelms-Universität Münster, Münster, Germany
⁵⁶ Institut Pluridisciplinaire Hubert Curien (IPHC), Université de Strasbourg, CNRS-IN2P3, Strasbourg, France
⁵⁷ Institute for Nuclear Research, Academy of Sciences, Moscow, Russia
⁵⁸ Institute for Subatomic Physics of Utrecht University, Utrecht, Netherlands
⁵⁹ Institute for Theoretical and Experimental Physics, Moscow, Russia
⁶⁰ Institute of Experimental Physics, Slovak Academy of Sciences, Košice, Slovakia
⁶¹ Institute of Physics, Academy of Sciences of the Czech Republic, Prague, Czech Republic
⁶² Institute of Physics, Bhubaneswar, India
⁶³ Institute of Space Science (ISS), Bucharest, Romania
⁶⁴ Instituto de Ciencias Nucleares, Universidad Nacional Autónoma de México, Mexico City, Mexico
⁶⁵ Instituto de Física, Universidad Nacional Autónoma de México, Mexico City, Mexico
⁶⁶ iThemba LABS, National Research Foundation, Somerset West, South Africa
⁶⁷ Joint Institute for Nuclear Research (JINR), Dubna, Russia
⁶⁸ Konkuk University, Seoul, South Korea
⁶⁹ Korea Institute of Science and Technology Information, Daejeon, South Korea
⁷⁰ KTO Karatay University, Konya, Turkey
⁷¹ Laboratoire de Physique Corpusculaire (LPC), Clermont Université, Université Blaise Pascal, CNRS-IN2P3, Clermont-Ferrand, France
⁷² Laboratoire de Physique Subatomique et de Cosmologie, Université Grenoble-Alpes, CNRS-IN2P3, Grenoble, France
⁷³ Laboratori Nazionali di Frascati, INFN, Frascati, Italy
⁷⁴ Laboratori Nazionali di Legnaro, INFN, Legnaro, Italy
⁷⁵ Lawrence Berkeley National Laboratory, Berkeley, CA, United States
⁷⁶ Moscow Engineering Physics Institute, Moscow, Russia
⁷⁷ Nagasaki Institute of Applied Science, Nagasaki, Japan
⁷⁸ National Centre for Nuclear Studies, Warsaw, Poland
⁷⁹ National Institute for Physics and Nuclear Engineering, Bucharest, Romania
⁸⁰ National Institute of Science Education and Research, Bhubaneswar, India
⁸¹ National Research Centre Kurchatov Institute, Moscow, Russia
⁸² Niels Bohr Institute, University of Copenhagen, Copenhagen, Denmark
⁸³ Nikhef, Nationaal instituut voor subatomaire fysica, Amsterdam, Netherlands
⁸⁴ Nuclear Physics Group, STFC Daresbury Laboratory, Daresbury, United Kingdom
⁸⁵ Nuclear Physics Institute, Academy of Sciences of the Czech Republic, Řež u Prahy, Czech Republic
⁸⁶ Oak Ridge National Laboratory, Oak Ridge, TN, United States
⁸⁷ Petersburg Nuclear Physics Institute, Gatchina, Russia
⁸⁸ Physics Department, Creighton University, Omaha, NE, United States
⁸⁹ Physics Department, Panjab University, Chandigarh, India
⁹⁰ Physics Department, University of Athens, Athens, Greece
⁹¹ Physics Department, University of Cape Town, Cape Town, South Africa
⁹² Physics Department, University of Jammu, Jammu, India
⁹³ Physics Department, University of Rajasthan, Jaipur, India
⁹⁴ Physik Department, Technische Universität München, Munich, Germany
⁹⁵ Physikalisches Institut, Ruprecht-Karls-Universität Heidelberg, Heidelberg, Germany
⁹⁶ Purdue University, West Lafayette, IN, United States
⁹⁷ Pusan National University, Pusan, South Korea
⁹⁸ Research Division and ExtreMe Matter Institute EMMI, GSI Helmholtzzentrum für Schwerionenforschung, Darmstadt, Germany
⁹⁹ Rudjer Bošković Institute, Zagreb, Croatia
¹⁰⁰ Russian Federal Nuclear Center (VNIIEF), Sarov, Russia
¹⁰¹ Saha Institute of Nuclear Physics, Kolkata, India
¹⁰² School of Physics and Astronomy, University of Birmingham, Birmingham, United Kingdom
¹⁰³ Sección Física, Departamento de Ciencias, Pontificia Universidad Católica del Perú, Lima, Peru
¹⁰⁴ Sezione INFN, Bari, Italy
¹⁰⁵ Sezione INFN, Bologna, Italy
¹⁰⁶ Sezione INFN, Cagliari, Italy
¹⁰⁷ Sezione INFN, Catania, Italy
¹⁰⁸ Sezione INFN, Padova, Italy
¹⁰⁹ Sezione INFN, Rome, Italy
¹¹⁰ Sezione INFN, Trieste, Italy
¹¹¹ Sezione INFN, Turin, Italy
¹¹² SSC IHEP of NRC Kurchatov institute, Protvino, Russia
¹¹³ Stefan Meyer Institut für Subatomare Physik (SMI), Vienna, Austria

- 114 SUBATECH, Ecole des Mines de Nantes, Université de Nantes, CNRS-IN2P3, Nantes, France
115 Suranaree University of Technology, Nakhon Ratchasima, Thailand
116 Technical University of Košice, Košice, Slovakia
117 Technical University of Split, FESB, Split, Croatia
118 The Henryk Niewodniczanski Institute of Nuclear Physics, Polish Academy of Sciences, Cracow, Poland
119 The University of Texas at Austin, Physics Department, Austin, TX, United States
120 Universidad Autónoma de Sinaloa, Culiacán, Mexico
121 Universidade de São Paulo (USP), São Paulo, Brazil
122 Universidade Estadual de Campinas (UNICAMP), Campinas, Brazil
123 University of Houston, Houston, TX, United States
124 University of Jyväskylä, Jyväskylä, Finland
125 University of Liverpool, Liverpool, United Kingdom
126 University of Tennessee, Knoxville, TN, United States
127 University of the Witwatersrand, Johannesburg, South Africa
128 University of Tokyo, Tokyo, Japan
129 University of Tsukuba, Tsukuba, Japan
130 University of Zagreb, Zagreb, Croatia
131 Université de Lyon, Université Lyon 1, CNRS/IN2P3, IPN-Lyon, Villeurbanne, France
132 Università di Brescia, Italy
133 V. Fock Institute for Physics, St. Petersburg State University, St. Petersburg, Russia
134 Variable Energy Cyclotron Centre, Kolkata, India
135 Warsaw University of Technology, Warsaw, Poland
136 Wayne State University, Detroit, MI, United States
137 Wigner Research Centre for Physics, Hungarian Academy of Sciences, Budapest, Hungary
138 Yale University, New Haven, CT, United States
139 Yonsei University, Seoul, South Korea
140 Zentrum für Technologietransfer und Telekommunikation (ZTT), Fachhochschule Worms, Worms, Germany

i Deceased.

ii Also at: Georgia State University, Atlanta, Georgia, United States.

iii Also at: Department of Applied Physics, Aligarh Muslim University, Aligarh, India.

iv Also at: M.V. Lomonosov Moscow State University, D.V. Skobeltsyn Institute of Nuclear Physics, Moscow, Russia.